

Diffraction in time of polymer particles

A. Martín-Ruiz*

*Instituto de Ciencias Nucleares, Universidad Nacional Autónoma de México,
04510 México, Distrito Federal, Mexico*

(Received 12 June 2014; published 24 December 2014)

We study the quantum dynamics of a suddenly released beam of particles using a background independent (polymer) quantization scheme. We show that, in the first order of approximation, the low-energy polymer distribution converges to the standard quantum-mechanical result in a clear fashion, but also arises an additional small polymer correction term. We find that the high-energy polymer behavior becomes predominant at short distances and short times, as we should expect. Numerical results are also presented. We find that particles whose wave functions satisfy the polymer wave equation do not exhibit the diffraction in time phenomena. The implementation of a modified time-energy uncertainty relation in the polymer framework is briefly discussed.

DOI: 10.1103/PhysRevD.90.125027

PACS numbers: 03.65.-w, 04.60.Ds, 04.60.Pp

I. INTRODUCTION

One of the main challenges in physics today is the search for a quantum theory of gravity (QTG). A major difficulty in the development of such theories is the lack of experimentally accessible phenomena that could shed light on the possible route to QTG. Such quantum gravitational effects are expected to become relevant near the Planck scale, where spacetime itself is assumed to be quantized. Compared to the typical energy scales we are able to reach in our experiments, the Planck energy is extremely high, too high to hope to be able to test it directly, which makes it so difficult to test such effects.

Because the predictions of quantum mechanics have been verified experimentally to an extremely high degree of accuracy, a possible route to test quantum gravitational effects is through high-sensitivity measurements of well known quantum-mechanical phenomena, as any deviation from the standard theory is, at least in principle, experimentally testable. In this framework, with the best position measurements (being of the order $\Delta x \sim 10^{-18}$ m), at present sensitivities are still insufficient and quantum gravitational corrections remain unexplored. Despite this limitation, experimental verification of a common modification of the Heisenberg uncertainty relation that appears in a vast range of approaches to QTG has been reported in [1].

A background independent quantization scheme that arose in loop quantum gravity (LQG), the so-called polymer quantization (PQ), has been used to explore mathematical and physical implications of theories such as quantum gravity [2,3]. PQ may be viewed as a separate development in its own right and is applicable to any classical theory whether it contains or does not contain gravity. Its central feature is that the momentum operator p is not realized directly as in Schrödinger quantum

mechanics because of a built-in notion of discreteness but arises indirectly through the translation operator $U_\lambda \equiv e^{i\frac{p\lambda}{\hbar}}$. Various approaches to QTG (such as LQG, string theory, and noncommutative geometries) suggest the existence of a minimum measurable length or a maximum observable momentum [4–6]. In PQ a length scale is required for its construction, while for the gravitational case this is identified with Planck length, and in the mechanical case it is just a free parameter.

In this paper we analyze the physical consequences of the PQ scheme in the dynamics of a well-known quantum transient phenomena: diffraction in time (DIT). DIT was discussed first by Moshinsky [7]. It is a phenomenon associated with the quantum dynamics of suddenly released quantum particles initially confined in a region of space.¹ The hallmark of DIT consists of temporal and spatial oscillations of the quantum density profile [8]. The basic results of Moshinsky's shutter are reviewed in Appendix A. In Sec. II we consider the shutter problem in the framework of polymer quantum mechanics. In Sec. III we show that the polymer result converges to the Moshinsky result in the appropriate limit. In Sec. IV we demonstrate that no DIT effect arises when the wave function satisfies the polymer wave equation. Finally in Sec. V we briefly discuss the implementation of a modified time-energy uncertainty relation in the polymer framework.

II. THE SHUTTER PROBLEM IN POLYMER QUANTUM MECHANICS

The problem we shall discuss is the following: a monochromatic beam of polymer particles of mass m and momentum $p > 0$ impinges on a totally absorber

¹The original setting consisted of a sudden opening of a shutter to release a semi-infinite beam and provided a quantum, temporal analogue of spatial Fresnel diffraction theory by a sharp edge.

*alberto.martin@nucleares.unam.mx

shutter located at the origin. If at $t = 0$ the shutter is opened, what will be the transient polymer density profile at a distance x_μ from the shutter?

To tackle this problem, we first restrict the dynamics to an equispaced lattice $\gamma(\lambda) = \{\lambda n | n \in \mathbb{Z}\}$. The spectrum of the position operator $\{x_\mu = \lambda\mu\}$ consists of a countable selection of points from the real line, which is analogous to the graphs covering 3-manifolds in LQG. The polymer Hilbert space H_{poly}^2 consists of position wave functions that are nonzero only on the lattice, restricting the momentum wave functions to be periodic functions of period $\frac{2\pi\hbar}{\lambda}$ [9,10]. Here λ is regarded as a fundamental length scale of the polymer theory.

[For a simpler analysis of the problem, hereafter we use the following dimensionless quantities for position, momentum, energy, and time:

$$\mu \equiv \frac{x_\mu}{\lambda}, \quad \rho \equiv \frac{p\lambda}{\hbar}, \quad \varepsilon \equiv \frac{m\lambda^2 E}{\hbar^2}, \quad \tau \equiv \frac{\hbar t}{m\lambda^2}, \quad (1)$$

respectively. Also we use the notation $\psi_\mu(\tau) \equiv \psi(x_\mu, \tau)$ for the wave function in coordinate representation.]

For (nonrelativistic) polymer particles, the wave function $\psi_\mu(\tau)$ that represents the state of the beam of polymer particles for $\tau > 0$ satisfies the time-dependent polymer Schrödinger equation [11,12]

$$2i \frac{\partial}{\partial \tau} \psi_\mu(\tau) = 2\psi_\mu(\tau) - \psi_{\mu+1}(\tau) - \psi_{\mu-1}(\tau) \quad (2)$$

and the initial wave function

$$\psi_\mu(\tau = 0) = e^{i\rho\mu} \Theta(-\mu), \quad (3)$$

where $\Theta(y)$ is the Heaviside step function, and the momentum $\rho \in [0, \pi)$ is a solution of the (free) polymer dispersion relation, $\varepsilon(\rho) = 1 - \cos \rho$, considering a fixed value of ε . Note that the energy spectrum is bounded from above, and the bound depends on the length scale λ .

For $\tau > 0$ the shutter has been removed and the dynamics is free. By using the free polymer propagator [13], namely

$$K_\lambda(\mu, \tau; \nu, \tau_0) = i^{\nu-\mu} J_{\nu-\mu}(\tau - \tau_0) e^{-i(\tau-\tau_0)}, \quad (4)$$

the solution of (2), subject to the initial condition (3), is then

$$\psi_\mu(\tau) = e^{-i(\tau-\rho\mu)} \Phi_\mu(\rho, \tau), \quad (5)$$

²The kinematical Hilbert space can be written as $H_{\text{poly}} = L^2(\mathbb{R}_d, d\mu_d)$, with $d\mu_d$ the corresponding Haar measure and \mathbb{R}_d the real line endowed with the discrete topology.

where we have defined

$$\Phi_\mu(\rho, \tau) \equiv \sum_{\nu=-\infty}^{-\mu} J_\nu(\tau) e^{i(\rho+\frac{\pi}{2})\nu}, \quad (6)$$

By using properties of Bessel functions, one can further check that $\psi_\mu(\tau)$ satisfies (2) and the initial condition (3).

The corresponding polymer density profile,

$$|\psi_\mu(\tau)|^2 = \sum_{\nu, \alpha=-\infty}^{-\mu} J_\nu(\tau) J_\alpha(\tau) \cos \left[\left(\rho + \frac{\pi}{2} \right) (\nu - \alpha) \right], \quad (7)$$

cannot be reduced to a simple form but can be treated numerically. Plots of the polymer and the Moshinsky density profiles for both the low and the high energy regimes are presented in Figs. 1 and 2, respectively. At low energies ($\rho \ll 1$) the polymer and standard cases behave qualitatively in a similar manner. However, at high energies the polymer distribution exhibits some differences with

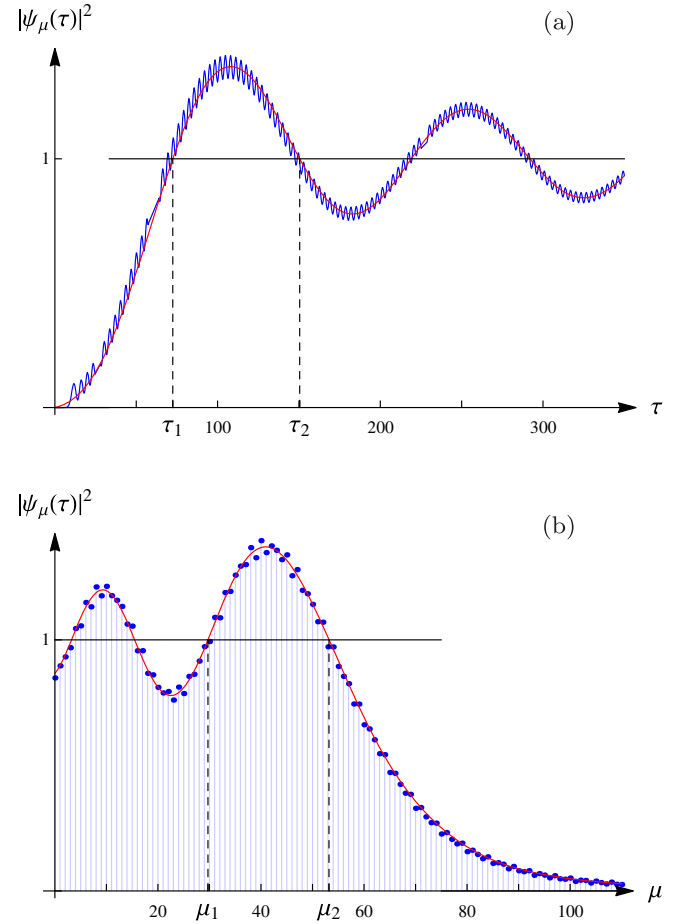


FIG. 1 (color online). The low energy ($\rho = 0.3$) polymer density profile (a) as a function of time τ at a fixed distance x_{10} [solid (blue) line], and (b) as a function of μ at a fixed time $\tau = 250$ [discrete (blue) plot]. In both (a) and (b) the solid (red) line corresponds to the Moshinsky distribution, and the solid (black) line corresponds to the classical result.

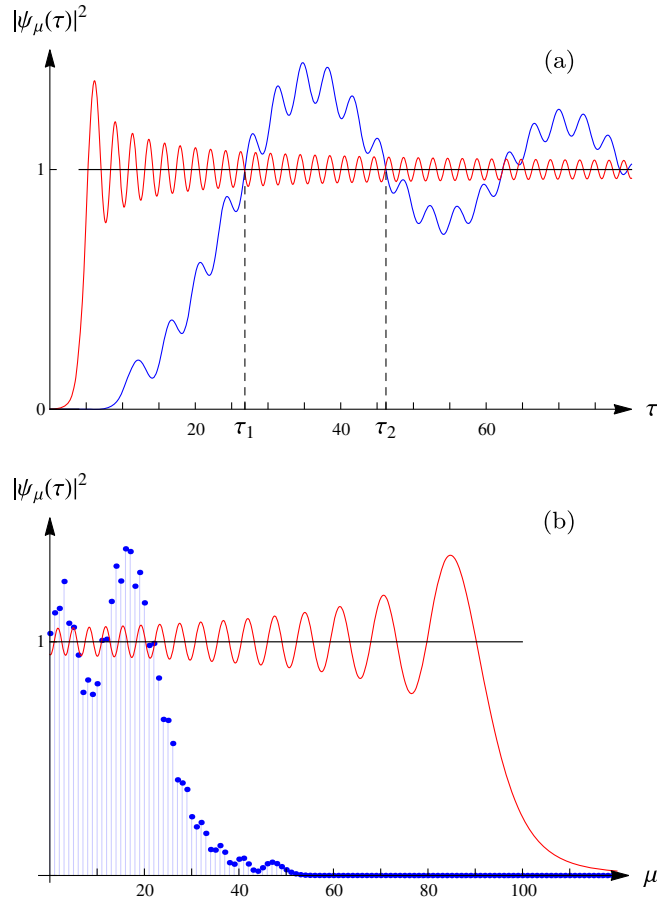


FIG. 2 (color online). The high energy ($\rho = 2.5$) polymer density profile (a) as a function of time τ at a fixed distance x_{10} [solid (blue) line], and (b) as a function of μ at a fixed time $\tau = 50$ [discrete (blue) plot]. In both (a) and (b) the solid (red) line corresponds to the Moshinsky distribution, and the solid (black) line corresponds to the classical result.

respect to the standard case. Next we discuss the aforementioned limiting cases.

In Fig. 1(a) we plot the low energy polymer distribution as a function of time τ at a fixed distance x_μ . We observe that the polymer result exhibits small oscillations superimposed on the Moshinsky result. This situation resembles the quantum-classical transition problem, where the classical distribution follows the spatial local average of the quantum probability density for large quantum numbers [14,15]. In this framework, Fig. 1(a) suggests that the polymer and quantum-mechanical distributions approach each other in a locally time-averaged sense at low energies.

As in the standard case, a good measure of the width of the polymer diffraction effect in time can be obtained from the difference $\delta\tau$ between the first two times at which $|\psi_\mu(\tau)|^2$ takes the classical value 1, i.e., $\delta\tau = \tau_2 - \tau_1$, as shown in Fig. 1(a). In this case such a time difference can be estimated the same way as in the quantum-mechanical case (see Appendix A) because at first order of approximation, the low-energy polymer wave function converges

to the Moshinsky function evaluated on points in the lattice, i.e., $\psi_\mu(\tau) \sim M(x_\mu, p, t)$ [see Eq. (19)] By using the Cornu spiral [16] one obtains

$$\delta\tau \approx 0.85 \sqrt{\frac{\pi\mu}{\rho^3}}, \quad (8)$$

for $\rho\mu \gg 1$, in agreement with the results of Fig. 1(a).

In Fig. 1(b) we present the low energy polymer density profile as a function of μ at a fixed time τ . As expected, we observe that the polymer result (discrete blue plot) resembles the standard result (continuous red line) as increasing μ , showing oscillations near the edge. The width of these oscillations can also be estimated the same way as in the standard case (see Appendix A). With the help of the Cornu spiral one obtains

$$\delta\mu = 0.85\sqrt{\pi\tau}. \quad (9)$$

It would be interesting to test whether these polymer corrections could be detected with high sensitivity experiments for the case of real quantum systems approaching the quantum-polymer boundary. Currently, with the best position measurements [1] no quantum gravity effect has been detected in laboratory experiments, and therefore it represents an upper bound on the fundamental length scale (at present $\lambda \ll 10^{-18}$ m). In the problem at hand, the experimental verification of Moshinsky's DIT phenomenon presents several difficulties. In addition to the feebleness of such an effect, dissipation, environmental noise, and repulsive interatomic interactions tend to suppress it. Currently, no DIT fringes on the density profile have been observed, but recent developments of a guided atom laser [17] open such a possibility. Regarding the polymer corrections to Moshinsky's density profile, the difference between both distributions, $P(x_\mu, \tau) = |\psi_\mu(\tau)|^2 - |M(x_\mu, p, t)|^2$, represents a good measure of the residual polymer behavior at quantum level; however, at low energies such a difference is of the order of the fundamental length scale of the theory, as we can see in Eq. (19). Therefore at present the polymer corrections to the density profile are virtually impossible to detect in the lab.

The analysis in Ref. [18] points out that the experimental observation of quantum transients would be simpler for time-energy uncertainty relation than for interference effects on the density profile. In this framework, a series of experiments [19,20] has culminated in the confirmation of the time-energy uncertainty relation for pulse formation predicted by Moshinsky [21]. It would be interesting to study the pulse formation of polymer particles in order to establish a modified time-energy uncertainty relation that could be tested in the lab. In Sec. V we briefly discuss the pulse formation, and we establish the starting point for its analysis in polymer quantum mechanics.

The high energy polymer density profile as a function of time τ at fixed distance x_μ is presented in Fig. 2(a). Clearly,

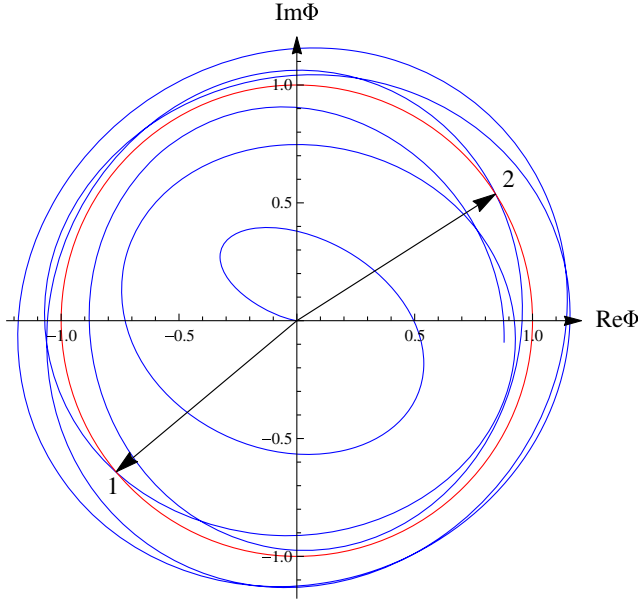


FIG. 3 (color online). Parametric like spiral for $\Phi_{10}(2.5, \tau)$.

this case does not admit a simple analysis in terms of the Cornu spiral because the polymer distribution differs significantly with respect to the Moshinsky result. However, we can construct a parametric like spiral to perform a similar analysis. The standing point is that the polymer distribution can be expressed as $|\text{Re}\Phi|^2 + |\text{Im}\Phi|^2$, where Im and Re stand for the imaginary and real parts of the function Φ (6), respectively. Therefore we consider the curve that results from the parametric representation $(\text{Re}\Phi, \text{Im}\Phi)$. In the like-spiral diagram of Fig. 3, the polymer probability density (7) is the square of the radius vector from the origin $(0,0)$ to the point on the spiral whose distance from the origin, along the curve, is τ . For the case considered in Fig. 2(a), when τ goes from 0 to the classical time of flight $\tau_{\text{cl}} = \frac{\mu}{\rho}$, the polymer distribution increases very slowly from 0 to 4.71×10^{-8} . In other words, the classical time τ_{cl} is very small for detecting time-diffracted polymer particles.

The times at which the polymer distribution intersects the classical value 1 correspond to the values of τ obtained from the intersection of the like-spiral diagram with the circle of radius 1 and center $(0,0)$ in Fig. 3. The values of τ_2 and τ_1 are the lengths along the like spiral from the origin to points 1 and 2 in Fig. 3, so that we have $\delta\tau \approx 19$, in agreement with that presented in Fig. 2(a). Of course, as the energy increases, the time width $\delta\tau$ increases, but also it is the first time τ_1 the polymer distribution takes the classical value. Therefore high energy polymer particles also exhibit the diffraction effect in time, but with the characteristic times (τ_1 and $\delta\tau$) increased. In the limiting case $\rho \rightarrow \pi$ the time τ_1 tends to infinite, and then the polymer particles (with the maximum possible energy) do not exhibit the diffraction effect in time. In the like-spiral diagram of

Fig. 3, this case looks like a dense spiral completely contained in the unit circle.

In Fig. 2(b) we plot the high energy polymer distribution as a function of μ at a fixed time τ . We observe that the polymer distribution decreases abruptly before the particles reach the edge and that the μ_2 value is smaller than for low energy polymer particles. Physically our results imply that the high energy polymer effects become important at short distances [Fig. 2(b)] and short times [Fig. 2(a)], as expected. If quantum gravitational effects become relevant near the Planck scale, as commonly believed, the energy needed for detecting high energy time-diffracted particles is of the order of Planck energy, which is extremely high compared with the energies we are able to reach in our experiments.

III. THE POLYMER-SCHRÖDINGER TRANSITION

It has been argued that if the lattice spacing λ is taken to be sufficiently small, the polymer formulation should reduce to the Schrödinger representation [12]. This is a delicate issue because λ is regarded as a nonzero fundamental length scale of the polymer theory, and it cannot be removed when working in H_{poly} , no matter how small λ is. This is analogous to the quantum-classical transition problem through the $\hbar \rightarrow 0$ limit, because \hbar is a nonzero fundamental constant of the quantum theory [14,15].

To address the polymer-Schrödinger transition, we consider the low energy regime of the polymer theory ($\rho \ll 1$) that one expects to be the domain of validity of the Schrödinger theory. Clearly, the standard energy spectrum is recovered in the $\rho \ll 1$ limit,

$$E(p) \approx \frac{p^2}{2m} \ll \frac{2\hbar^2}{m\lambda^2}, \quad (10)$$

but it remains bounded from above due to nonzero λ . In terms of the de Broglie wavelength $\lambda_{\text{DB}} = \frac{2\pi\hbar}{p}$, this limit can be expressed as $\lambda \ll \lambda_{\text{DB}}$; i.e., the fundamental length is very small compared with the characteristic quantum-mechanical length. Taking λ in the order of the Planck length, the typical diffraction experiments of electrons and neutrons, for which $\lambda_{\text{DB}} \sim 10^{-10}$ m, strongly satisfy the required condition [13].

Physically the $\lambda \ll \lambda_{\text{DB}}$ limit implies that we should take a very large number of points between two arbitrary points, but keep its distance fixed. Consequently for the distance between the shutter and the observer we must consider $\mu \gg 1$, and then the asymptotic behavior of Bessel functions for large indices in Fig. 5 is required. On the other hand, the time needed for the particle to move from x_ν to x_μ with momentum p is $\tau = \frac{|\mu-\nu|}{p}$. Then by keeping the distance fixed, the $\rho \ll 1$ limit implies that $\tau \gg 1$, and therefore the asymptotic behavior of (5) for large values of τ is also required. Note that the argument of the Bessel

function grows faster than its order, so that the $\tau \gg 1$ limit will dominate the transition [13].

The asymptotic expansion of the Bessel functions for large arguments is well known [21]. It can be written as

$$J_\nu(\tau) \sim \frac{e^{i[\tau - \frac{\pi}{2}(\nu + \frac{1}{2})]}}{\sqrt{2\pi\tau}} \{R_\nu(\tau) + R_\nu^*(\tau)e^{-2i[\tau - \frac{\pi}{2}(\nu + \frac{1}{2})]}\}, \quad (11)$$

where $R_\nu(\tau) \equiv P_\nu(\tau) + iQ_\nu(\tau)$, with

$$P_\nu(\tau) = \sum_{n=0}^{\infty} \frac{(-1)^n}{(2n)!(2z)^{2n}} \frac{\Gamma(\nu + 2n + \frac{1}{2})}{\Gamma(\nu - 2n + \frac{1}{2})},$$

$$Q_\nu(\tau) = \sum_{n=0}^{\infty} \frac{(-1)^n}{(2n+1)!(2z)^{2n+1}} \frac{\Gamma(\nu + (2n+1) + \frac{1}{2})}{\Gamma(\nu - (2n+1) + \frac{1}{2})}. \quad (12)$$

We observe that the expression (11) depends on the order of the Bessel function through both the exponentials and the Gamma functions in (12). Fortunately only the second one becomes important for large indices $\nu \gg 1$. Using the approximation $\frac{\Gamma(\nu+a+\frac{1}{2})}{\Gamma(\nu-a+\frac{1}{2})} \sim \nu^{2a}$ for $\nu \gg 1$, the function $R_\nu(\tau)$ becomes

$$R_\nu(\tau) \sim e^{i\frac{\pi}{2\nu}}. \quad (13)$$

Finally the asymptotic behavior of the Bessel function $J_\nu(\tau)$, for large arguments ($\tau \gg 1$) and large orders ($\nu \gg 1$), yields

$$J_\nu(\tau)e^{-i\tau + i\frac{\pi\nu}{2}} \sim \frac{e^{-i\frac{\pi}{4}}}{\sqrt{2\pi\tau}} \{e^{i\frac{\nu^2}{2\tau}} + i(-1)^\nu e^{-i\frac{\nu^2}{2\tau} - 2i\tau}\}. \quad (14)$$

One can further check that in this regime the term proportional to $e^{-2i\tau}$ makes no contribution to the asymptotic behavior because it produces a distributional expression, as pointed out in Ref. [13].

Substituting (14) in (5) we get a discrete version of the Moshinsky function,

$$\psi_\mu(\tau) \sim m(x_\mu, p, t) \equiv e^{i(\rho\mu - \frac{\rho^2\tau}{2})} \frac{e^{-i\frac{\pi}{4}}}{\sqrt{2\pi\tau}} \sum_{\nu=-\infty}^{\rho\tau-\mu} e^{i\frac{\nu^2}{2\tau}}, \quad (15)$$

which satisfies analogous properties [8], i.e.,

- (i) Under inversion of both x_μ and p , it satisfies

$$m(x_\mu, p, t) + m(-x_\mu, -p, t) = e^{i(\rho\mu - \frac{\rho^2\tau}{2})} \vartheta_3(0, -2\pi\tau), \quad (16)$$

where ϑ_3 is Jacobi's elliptic theta function [22].

- (ii) The asymptotic behavior for $|\rho\tau - \mu| \rightarrow \infty$ and $\rho\tau \geq \mu$ is

$$m(x_\mu, p, t) \sim e^{i(\rho x_\mu - \frac{\rho^2 t}{2m})}, \quad (17)$$

which is the standard quantum-mechanical result: a plane wave traveling to the right with momentum p and energy $\frac{p^2}{2m}$.

- (iii) It satisfies the polymer Schrödinger equation (2).

To illuminate the correspondence between $m(x_\mu, p, t)$ and the Moshinsky function (A4) in a clear fashion, we first approximate the sum in (6) by using the Euler-Maclaurin formula,

$$\Phi_\mu(\rho, \tau) \approx \int_{-\infty}^{-\mu} J_\nu(\tau) e^{i(\rho + \frac{\pi}{2})\nu} d\nu + \frac{1}{2} J_{-\mu}(\tau) e^{-i(\rho + \frac{\pi}{2})\mu}, \quad (18)$$

where we have used that $J_\nu(\tau) \rightarrow 0$ as $\nu \rightarrow \infty$. Now, by the use of the asymptotic expansion of Bessel functions (14) we obtain

$$m(x_\mu, p, t) \cong \frac{e^{-i\frac{\pi}{4}}}{\sqrt{2}} e^{i(\rho x_\mu - \frac{p^2}{2m}t)} \left\{ \left[\frac{1}{2} + C(\xi) \right] + i \left[\frac{1}{2} + S(\xi) \right] \right\} + \frac{1}{\sqrt{8\pi\tau}} e^{-i(\frac{\pi}{4} + \frac{\mu^2}{2\tau})}, \quad (19)$$

where $\xi \equiv \frac{1}{\sqrt{\pi\tau}}(\rho\tau - \mu) = \sqrt{\frac{m}{\pi\hbar^2}}(\frac{pt}{m} - x_\mu)$. We recognize the first term in (19) as the Moshinsky function (independent of λ) evaluated on points in the lattice, i.e., $M(x_\mu, p, t)$. The second term is small because it depends on $\frac{1}{\sqrt{\tau}} \ll 1$ but it is nonzero. Of course, this additional term represents the polymer residual behavior at quantum level. In this framework at low energies we can neglect the correction term to analyze the polymer behavior by using the Cornu spiral.

IV. POLYMER WAVE EQUATION

One may wonder if DIT takes place for different wave equations, such as the ordinary wave equation and the Klein-Gordon equation. In this framework Moshinsky showed that the DIT phenomenon arises only for the Schrödinger equation [7]. This is because only for the time-dependent Schrödinger equation is there an analogy with the phenomena of electromagnetic diffraction, which has to do with the resemblance that the solutions have with those that appear in Sommerfeld's theory of diffraction.

In this section we shall consider the shutter problem, but we assume that the state $\psi_\mu(\tau)$ satisfies the polymer wave equation

$$\frac{\partial^2 \psi_\mu(\tau)}{\partial \tau^2} = \psi_{\mu+1}(\tau) + \psi_{\mu-1}(\tau) - 2\psi_\mu(\tau), \quad (20)$$

where $\tau \equiv \frac{ct}{\lambda}$, and c is the speed of light. As usual, we will consider that initially ψ_μ and its time derivative are given by

$$\psi_\mu(0) = F_\mu, \quad \left(\frac{\partial \psi_\mu(\tau)}{\partial \tau} \right)_{\tau=0} = G_\mu. \quad (21)$$

The solution of (20) can be obtained by using the Fourier integral theorem, i.e.,

$$\psi_\mu(\tau) = \frac{1}{2\pi} \int_{-\pi}^{+\pi} d\kappa \left[f(\kappa) \cos(\varepsilon_\kappa \tau) + g(\kappa) \frac{\sin(\varepsilon_\kappa \tau)}{\varepsilon_\kappa} \right] e^{i\kappa\mu}, \quad (22)$$

where $f(\kappa)$ and $g(\kappa)$ are the Fourier transforms of F_μ and G_μ , and $\varepsilon_\kappa = \sqrt{2(1 - \cos \kappa)}$. One can further check that $\psi_\mu(\tau)$ satisfies the polymer wave equation (20) and the initial conditions (21).

For $\tau < 0$ the shutter was closed, and then we had on the left side of the shutter the simple (truncated) plane wave solution

$$\psi_\mu(\tau) = e^{i(\rho\mu - \varepsilon_\rho \tau)} \Theta(-\mu). \quad (23)$$

This implies that at $\tau = 0$ we have

$$F_\mu = e^{i\rho\mu} \Theta(-\mu), \quad G_\mu = -i\varepsilon_\rho e^{i\rho\mu} \Theta(-\mu). \quad (24)$$

By Fourier transforming (24) we obtain that the initial conditions in the Fourier space become

$$\begin{aligned} f(\kappa) &= \pi \delta(\kappa - \rho) + i \cot(\kappa - \rho), \\ g(\kappa) &= -i\varepsilon_\rho f(\kappa). \end{aligned} \quad (25)$$

These formulas are derived in Appendix B 1. We observe that in the low energy regime $f(\kappa)$ reduces to the δ_+ function in a clear fashion.

Substituting (25) into (22) we get

$$\begin{aligned} \psi_\mu(\tau) &= \frac{1}{2} e^{i(\rho\mu - \varepsilon_\rho \tau)} - \frac{1}{4\pi i} \mathbf{p.v.} \int_{-\pi}^{+\pi} d\kappa \cot(\kappa - \rho) \\ &\quad \times \left\{ \left(1 + \frac{\varepsilon_\rho}{\varepsilon_\kappa} \right) e^{i(\kappa\mu - \varepsilon_\kappa \tau)} + \left(1 - \frac{\varepsilon_\rho}{\varepsilon_\kappa} \right) e^{i(\kappa\mu + \varepsilon_\kappa \tau)} \right\}. \end{aligned} \quad (26)$$

In this expression we interpret the integral in the sense of Cauchy's principal value. We observe that, as in the standard case, the integrand has a simple pole at $\kappa = \rho$ and an essential singularity at $\kappa = 0$; however, in (26) an additional simple pole also emerges at $\kappa = \rho - \pi$. As the lattice spacing is reduced, the solution of (26) becomes a simple task. In this regime, the limits of integration become from $-\infty$ to ∞ , the standard dispersion relation $\varepsilon_\kappa = \kappa$ is recovered, the initial condition $f(\kappa)$ becomes the δ_+ function, and the pole at $\rho - \pi$ does not take place. For such a case the principal value can be computed directly by using Cauchy's theorem. For the polymer case the integral becomes a difficult task, but it can be computed analytically. In Appendix B 2 we evaluate the principal value of the integral in (26). The result is

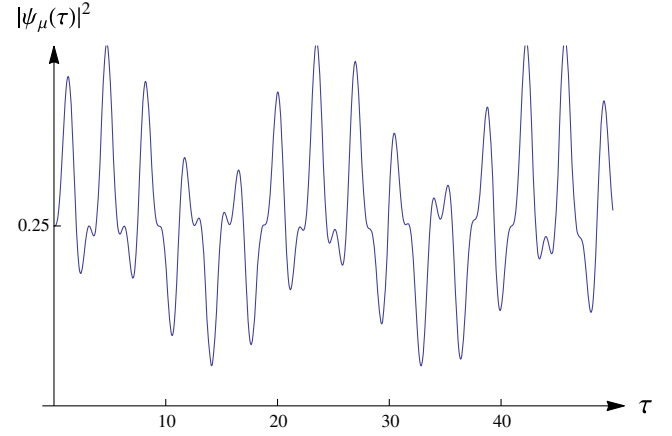


FIG. 4 (color online). Density profile for polymer wave equation as a function of time τ at a fixed distance $\mu = 10$.

$$\begin{aligned} \psi_\mu(\tau) &= \frac{1}{2} e^{i(\rho\mu - \varepsilon_\rho \tau)} + \frac{2}{\pi i} \sum_{\nu=-\infty}^{+\infty} \frac{J_{2\nu}(2\tau)}{\varsigma} \sin^2\left(\frac{\pi\varsigma}{2}\right) \\ &\quad \times \left[1 - {}_2F_1\left(1, -\frac{\varsigma}{2}; 1 - \frac{\varsigma}{2}, e^{2i\rho}\right) \Theta(-\varsigma) \right. \\ &\quad \left. - {}_2F_1\left(1, \frac{\varsigma}{2}; 1 + \frac{\varsigma}{2}, e^{-2i\rho}\right) \Theta(\varsigma) \right], \end{aligned} \quad (27)$$

where $\varsigma = \mu + \nu \neq 0$, J_n are the Bessel functions of first kind, and ${}_2F_1(a, b; c; z)$ are the Gauss hypergeometric functions in the unit circle $|z| = 1$. The Heaviside step functions in (27) ensure the convergence of the corresponding hypergeometric functions. In Fig. 4 we plot the density profile for the solution (27). We observe that the density profile is a simple oscillatory function, and this behavior certainly has no resemblance to the DIT effect obtained for the Schrödinger equation. For the Klein-Gordon equation the solution (26) still works, but with the dispersion relation $\varepsilon_\kappa^2 = 4\sin^2 \frac{\kappa}{2} + m'^2$, where $m' = \frac{m c \lambda}{\hbar}$. Of course, no DIT effect is expected. It would be interesting to study well-known phenomena for spin-0 particles in the polymer quantization scheme, e.g., polymer corrections to the energy spectrum of a π^- meson in a Coulomb potential.

V. DISCUSSION

The implications of the introduction of a nonzero fundamental length scale in quantum theory are quite profound. For example, the Heisenberg theorem, one of the cornerstones of quantum mechanics, states that the position x and momentum p of a particle cannot be simultaneously known with arbitrary precision, but the indeterminacies of a joint measurement are always bounded by $\Delta x \Delta p \geq \frac{\hbar}{2}$. The implementation of such a minimal length in quantum theory introduces a lower bound to the possible resolution of distances. It has therefore been suggested that the Heisenberg uncertainty relations should be modified to take into account the effects of spatial “grainy” structure [4–6].

In this framework, Generalized Uncertainty Principle (GUP) theories predict both a minimal observable length and a maximal momentum in the modified uncertainty relation $\Delta x \Delta p \geq \frac{\hbar}{2} [1 - 2\hbar^{-1} \Delta x_{\min} \Delta p + 4\hbar^{-2} (\Delta x_{\min} \Delta p)^2]$, with $2\Delta p_{\max} \sim \hbar (\Delta x_{\min})^{-1}$. The implementation of such ideas in polymer quantum mechanics is a difficult task because the momentum operator is not directly realized as in Schrödinger quantum mechanics; furthermore the polymer Hilbert space admits states with $\Delta x = 0$, and then the conventional uncertainty relations do not apply [23].

It is well known that ordinary diffraction phenomena for beams of particles are closely associated with the position-momentum uncertainty relation, and the appearance of diffraction in time effects are closely connected with the time-energy uncertainty relation $\Delta E \Delta t \geq \frac{\hbar}{2}$. The possibility of closing the shutter after a time Δt has been used to form a pulse. For small values of Δt the time-energy uncertainty relation comes into play, broadening the energy distribution of the resulting pulse [24]. In the problem at hand, the lower bound to the possible resolution of distances introduces a minimal temporal window for the pulse formation of polymer particles. Therefore we suggest that also the time-energy uncertainty relation must be modified to implement the nonzero minimal uncertainty in time. Since fringes in the density profile are difficult to detect in laboratory experiments, it would be interesting to study the pulse formation of polymer particles in order to establish such a modified time-energy uncertainty relation. Such analysis is beyond the scope of this paper, but we can establish the starting point. The probability for detecting a time diffracted polymer particle with energy $\varepsilon = 1 - \cos \rho$ at time $\Delta \tau$ after the beam is released is

$$P(\varepsilon, \varepsilon', \Delta \tau) = \left| \sum_{\mu} \varphi_{\mu}^*(\tau = 0) \psi_{\mu}(\Delta \tau) \right|^2, \quad (28)$$

where $\varphi_{\mu}(\tau = 0) = e^{i\rho'\mu} \Theta(-\mu)$ is the initial state of a particle with energy $\varepsilon' = 1 - \cos \rho'$, and $\psi_{\mu}(\Delta \tau)$ is given by Eq. (5). The resulting probability depends on both the time width $\Delta \tau$ and the energies ε and ε' . Therefore we can study the region for which $P(\varepsilon, \varepsilon', \Delta \tau)$ differs significantly from zero and then establish the corresponding modified time-energy uncertainty relation. Another possible extension of this work includes more complicated (time-dependent) shutter windows, focusing on the amplification of the residual polymer behavior at low energies.

The implementation of both the position-momentum and the time-energy modified uncertainty relations could play an important role in other branches of physics. For example, in the framework of local quantum field theories, the reason we have ultraviolet divergencies is that in the short time region $\Delta t \rightarrow 0$, the uncertainty with respect to energy increases indefinitely, $\Delta E \rightarrow \infty$, which in turn induces a large uncertainty in momentum Δp . The large uncertainty in momentum means that the particle states

allowed in the short distance region Δx grow indefinitely as $(\Delta E)^3$ in four-dimensional space-time [25]. In these theories where there is no built-in cutoff, all those states are expected to contribute to amplitudes with equal strength and consequently lead to UV infinities. A theory that naturally provides the adequate modified uncertainty relations could shed light on the route for curing such UV divergences.

Finally, let us summarize our results. In Sec. II we study the quantum dynamics of a suddenly released beam of polymer particles for both the low and the high energy regimes. Our numerical results show that in the quantum domain, the polymer distribution (as a function of time) exhibits small oscillations superimposed on the quantum-mechanical result [Fig. 1(a)]. Also the discrete spatial behavior resembles the standard result for long distances, as shown in Fig. 1(b). In Sec. III we show in an analytical clear fashion that in the first order of approximation the low energy polymer density profile converges to the Moshinsky distribution, but also emerges as an additional polymer correction term, responsible of the small temporal and spatial deviations in Fig. 1. At high energies the diffraction effect in time also takes place, but only for long times [see Fig. 2(a)]. For polymer particles with the maximum possible energy the DIT is no longer present. Regarding the spatial behavior, the polymer distribution decreases abruptly before the particles reach the edge, as shown in Fig. 2(b). As expected, the polymer effects become important at short distances and short times. On the other hand, we find that no diffraction effect in time arises when the wave functions satisfy the polymer wave equation.

ACKNOWLEDGMENTS

The author would like to thank L. F. Urrutia, A. Frank, A. Carbajal, J. Bernal, and E. Chan for useful discussions, comments, and suggestions. He also is indebted to the reviewers for their valuable comments and suggestions to improve the quality of the paper.

APPENDIX A: THE MOSHINSKY SHUTTER

In the original Moshinsky setup [7], a quasimonochromatic beam of nonrelativistic quantum particles of momentum p is incident upon a perfectly absorbing shutter located at the origin and perpendicular to the beam. If the shutter is suddenly removed at $t = 0$, what will be the transient density profile at a distance x from the shutter?

The initial wave function that we shall consider is

$$\psi(x, t = 0) = e^{i\frac{px}{\hbar}} \Theta(-x), \quad (A1)$$

where $\Theta(x)$ is the Heaviside step function. Note that the state is not really monochromatic due to the spatial truncation, besides that is clearly not normalized. Since

for $t > 0$ the shutter has been removed, the dynamics is free and the time-evolved wave function is

$$\psi(x, t) = \int_{-\infty}^{\infty} K(x, t; x', t' = 0) \psi(x', t' = 0) dx', \quad (\text{A2})$$

with the free propagator

$$K(x, t; x', t') = \sqrt{\frac{m}{2\pi i \hbar (t - t')}} e^{i \frac{m(x-x')^2}{2\hbar(t-t')}}. \quad (\text{A3})$$

The solution of (A2) with the initial wave function (A1) is known as Moshinsky functions,

$$M(x, p, t) = \frac{e^{-i\frac{\pi}{4}}}{\sqrt{2}} e^{\frac{i}{\hbar}(px - \frac{p^2 t}{2m})} \left\{ \left[\frac{1}{2} + C(\xi) \right] + i \left[\frac{1}{2} + S(\xi) \right] \right\}, \quad (\text{A4})$$

where $C(\xi)$ and $S(\xi)$ are the Fresnel integrals [16], and $\xi \equiv \sqrt{\frac{m}{\pi \hbar i}} (\frac{p t}{m} - x)$.

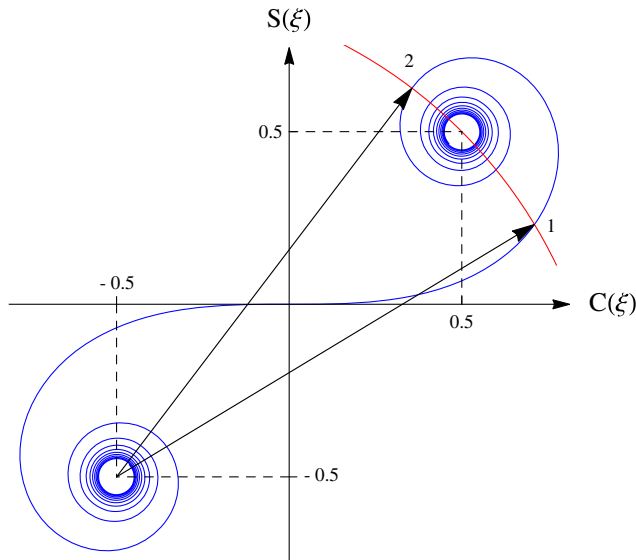


FIG. 5 (color online). Cornu spiral.

The “diffraction in time” term was introduced because the temporal behavior of the quantum density profile [see Fig. 6(a) below],

$$|M(x, p, t)|^2 = \frac{1}{2} \left\{ \left[\frac{1}{2} + C(\xi) \right]^2 + \left[\frac{1}{2} + S(\xi) \right]^2 \right\}, \quad (\text{A5})$$

admits a simple geometric interpretation in terms of Cornu spiral or clothoid, which is the curve that results from a parametric representation of the Fresnel integrals (Fig. 5). This is precisely the form of the intensity profile of a light beam diffracted by a semi-infinite plane [26], which prompted the choice of the DIT term. The probability density is one-half of the square of the distance from the point $(-\frac{1}{2}, -\frac{1}{2})$ to any other point of the Cornu spiral. In such a representation the origin corresponds to the classical particle with momentum p released at time $t = 0$ from the shutter position.

In Fig. 6(a) we present the classical and quantum density profiles at a fixed distance x as a function of time. The corresponding classical problem admits a trivial solution: the density profile vanishes if t is less than the time of flight $T = \frac{mx}{p}$, but one if $t \geq T$. On the other hand, with the help of the Cornu spiral we see that when t goes from 0 to T , the quantum density profile increases monotonically from 0 to $\frac{1}{4}$, while when t is larger than T , then $|M(x, k, t)|^2$ behaves as a damped oscillation around the classical value, tending to this value when $t \rightarrow \infty$.

The time width of this diffraction effect can be obtained from the difference δt between the first two times at which $|M(x, p, t)|^2$ takes the classical value, i.e., $\delta t = t_2 - t_1$, as shown in Fig. 6(a). Such times correspond to the values of ξ obtained from the intersection of the Cornu spiral with the circle of radius $\sqrt{2}$ and center $(-\frac{1}{2}, -\frac{1}{2})$. The difference $\delta \xi$ (that corresponds to δt) can be estimated as the arc length along the Cornu spiral between points 1 and 2 in Fig. 5, so that we have $\delta \xi = 0.85$. For $px \gg \hbar$ the result is

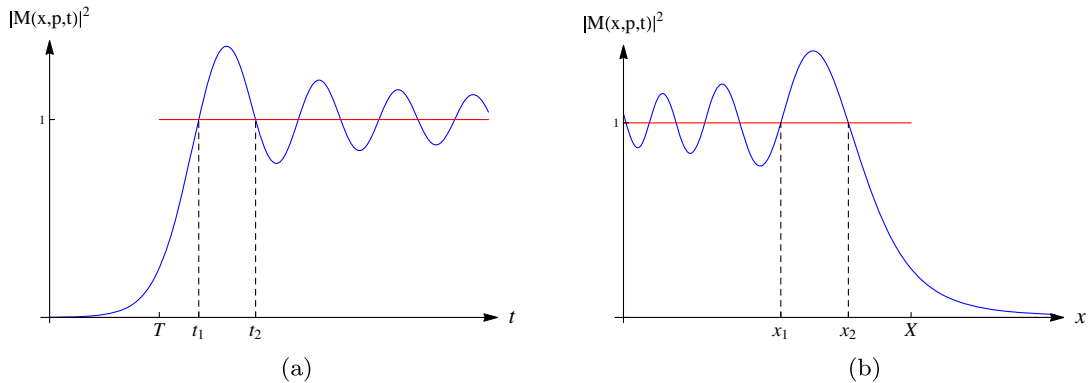


FIG. 6 (color online). Here we plot the classical (red line) and quantum (blue line) density profiles (a) as a function of time t at a fixed distance x , and (b) as a function of position x at a fixed time t .

$$\delta t \approx 0.85 \sqrt{\frac{\pi \hbar}{p x}} T. \quad (\text{A6})$$

Figure 6(b) shows the classical and quantum density profiles at a fixed time t as a function of position. We see that an initial sharp-edge wave packet will move with the classical velocity showing rapid oscillations near the edge, located at $X = \frac{p t}{m}$. As before, the width of these oscillations can be estimated through the distance δx between the first two values of x , starting from the edge, in which the probability density takes the classical value, i.e., $\delta x = x_2 - x_1$, as shown in Fig. 6(b). Using the Cornu spiral we obtain $\delta x = 0.85 \sqrt{\frac{\pi \hbar X}{p}}$.

A more general type of initial state has been considered,

$$\psi(x, t = 0) = e^{i \frac{p x}{\hbar}} + R e^{-i \frac{p x}{\hbar}}, \quad (\text{A7})$$

with $R = e^{i \pi \alpha}$ corresponding to a shutter with reflectivity $|R|^2 = 1$. Under free evolution, $\psi(x, t) = M(x, p, t) + R M(x, -p, t)$. For a complete review of the theory, results and experiments of quantum transients of single- to few-body systems see Ref. [8].

APPENDIX B: CALCULATIONS OF SEC. IV

1. Derivation of $f(\kappa)$ and $g(\kappa)$

Here we derive the initial conditions in momentum space by Fourier transforming (24), i.e.,

$$f(\kappa) = \sum_{\mu=-\infty}^{+\infty} \Theta(-\mu) e^{i(\rho-\kappa)\mu}. \quad (\text{B1})$$

To evaluate the sum, we consider the discretized derivative of the Heaviside step function,

$$\frac{\partial \Theta(\mu)}{\partial \mu} \approx \frac{1}{2} [\Theta(\mu + 1) - \Theta(\mu - 1)]. \quad (\text{B2})$$

Note that this expression is equivalent to two delta functions at $\mu = \pm 1$. Then we find that

$$\sum_{\mu=-\infty}^{+\infty} \frac{\partial \Theta(\mu)}{\partial \mu} e^{-i \zeta \mu} = \cos \zeta. \quad (\text{B3})$$

On the other hand, by substituting (B2) into (B3) and relabeling indices we find that

$$\sum_{\mu=-\infty}^{+\infty} \frac{\partial \Theta(\mu)}{\partial \mu} e^{-i \zeta \mu} = i \sin \zeta \sum_{\mu=-\infty}^{+\infty} \Theta(\mu) e^{-i \zeta \mu}. \quad (\text{B4})$$

By comparing (B3) and (B4) we obtain

$$\sum_{\mu=-\infty}^{+\infty} \Theta(\mu) e^{-i \zeta \mu} = -i \cot \zeta + \pi \delta(\zeta). \quad (\text{B5})$$

The π factor has been derived by using the property $\Theta(\mu) + \Theta(-\mu) = 1$. Finally with the help of (B5) we establish (25). The second initial condition is proportional to $f(\kappa)$.

2. The principal value

Here we shall evaluate the integral (26). To this end, first we rewrite the integral as simply as possible. By using the well-known Jacobi-Anger expansion [16] we get

$$\begin{aligned} \mathfrak{F} \equiv & \sum_{\nu=-\infty}^{+\infty} J_{\nu}(2\tau) \int_{-\pi}^{+\pi} d\kappa \cot(\kappa - \rho) e^{i \kappa \zeta} \\ & \times \left\{ [1 + (-1)^{\nu}] - [1 - (-1)^{\nu}] \sin \frac{\rho}{2} \csc \frac{\kappa}{2} \right\}, \quad (\text{B6}) \end{aligned}$$

where J_{ν} are the Bessel functions of first kind, and $\zeta \equiv \mu + \frac{\nu}{2}$. Note that the first integral in \mathfrak{F} is restricted to even values of ν (because it depends on $[1 + (-1)^{\nu}]$), while the second one is restricted to odd values of ν . We observe that the integrand has two simple poles at $\kappa = \rho, \rho - \pi$ and an essential singularity at $\kappa = 0$.

As the lattice spacing is reduced, the limits of integration become from $-\infty$ to ∞ , and then the pole at $\rho - \pi$ should not be considered. In this limiting case the principal value of \mathfrak{F} can be computed directly by using Cauchy's theorem. The case we consider is more subtle because momentum is defined in a bounded region, and therefore we should compute the principal value as usual.

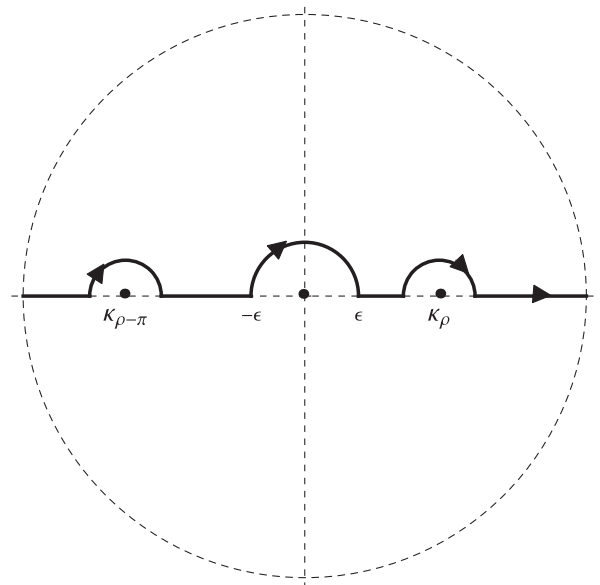


FIG. 7. κ plane.

We split the principal value of the integral \mathfrak{S} as follows:

$$\mathbf{p.v.}\mathfrak{S} = \lim_{\alpha,\epsilon,\beta \rightarrow 0^+} \left(\int_{-\pi}^{\rho-\pi-\alpha} + \int_{\rho-\pi+\alpha}^{-\epsilon} + \int_{+\epsilon}^{\rho-\beta} + \int_{\rho+\beta}^{\pi} \right) I dk, \quad (\text{B7})$$

where I is the integrand in (B6). See Fig. 7.

We obtain straightforwardly that the principal value of the even integral in \mathfrak{S} is

$$\begin{aligned} \mathfrak{S}_e &\equiv \mathbf{p.v.} \int_{-\pi}^{+\pi} dk \cot(\kappa - \rho) e^{i\kappa\zeta} \\ &= -\frac{4}{\zeta} \sin^2\left(\frac{\pi\zeta}{2}\right) \left[1 - {}_2F_1\left(1, -\frac{\zeta}{2}; 1 - \frac{\zeta}{2}; e^{2i\rho}\right) \Theta(-\zeta) \right. \\ &\quad \left. - {}_2F_1\left(1, \frac{\zeta}{2}; 1 + \frac{\zeta}{2}; e^{-2i\rho}\right) \Theta(\zeta) \right], \end{aligned} \quad (\text{B8})$$

where ${}_2F_1(a, b; c; z)$ are the hypergeometric Gauss functions in the unit circle $|z| = 1$. The Heaviside step functions in (B8) ensure the convergence of the corresponding hypergeometric functions.

On the other hand, we also obtain that the principal value of the odd integral in \mathfrak{S} is

$$\begin{aligned} \mathfrak{S}_o &\equiv \mathbf{p.v.} \int_{-\pi}^{+\pi} dk \cot(\kappa - \rho) \csc\left(\frac{\kappa}{2}\right) e^{i\kappa\zeta} \\ &= -2\pi i \cot \rho - 2 \cos(\pi\zeta) \cot \rho \left[e^{i\pi\zeta} (B(-i; 2\zeta, 0) + B(-i; 1 + 2\zeta, 0)) \right. \\ &\quad \left. - e^{-i\pi\zeta} (B(i; 2\zeta, 0) + B(i; 1 + 2\zeta, 0)) + 4i \tan \rho \left(\frac{{}_2F_1\left(1, \frac{1+2\zeta}{4}; \frac{5+2\zeta}{4}; e^{-2i\rho}\right)}{1 + 2\zeta} - \frac{{}_2F_1\left(1, \frac{3+2\zeta}{4}; \frac{7+2\zeta}{4}; e^{-2i\rho}\right)}{3 + 2\zeta} \right) \right], \end{aligned} \quad (\text{B9})$$

where $B(z; a, b)$ are the incomplete Beta functions in the unit circle. Here we have omitted the Heaviside functions that ensure the convergence of each term. Note that the second term in Eq. (B9) vanishes because $\cos(\pi\zeta) = 0$ for odd values of ν . Therefore only the first term in (B9) contributes to the integral. However, the substitution into Eq. (B8) vanishes because of the symmetry of Bessel functions. Therefore this odd term does not contribute to the principal value of \mathfrak{S} .

By substituting (B9) into (B7) we finally obtain that

$$\mathbf{p.v.}\mathfrak{S} = -8 \sum_{\nu=-\infty}^{+\infty} \frac{J_{2\nu}(2\tau)}{\zeta'} \sin^2\left(\frac{\pi\zeta'}{2}\right) \left[1 - {}_2F_1\left(1, -\frac{\zeta'}{2}; 1 - \frac{\zeta'}{2}; e^{2i\rho}\right) \Theta(-\zeta') - {}_2F_1\left(1, \frac{\zeta'}{2}; 1 + \frac{\zeta'}{2}; e^{-2i\rho}\right) \Theta(\zeta') \right] \quad (\text{B10})$$

with $\zeta' = \mu + \nu$. This result establishes (27).

-
- | | |
|--|---|
| <p>[1] I. Pikovski, M. R. Vanner, M. Aspelmeyer, M. S. Kim, and Č. Brukner, <i>Nat. Phys.</i> 8, 393 (2012).</p> <p>[2] G. M. Hossain, V. Husain, and S. S. Seahra, <i>Phys. Rev. D</i> 81, 024005 (2010).</p> <p>[3] G. Chacón-Acosta, E. Manrique, L. Dagdug, and H. A. Morales-Técotl, <i>SIGMA</i> 7, 100 (2011).</p> <p>[4] S. Hossenfelder, M. Bleicher, S. Hofmann, J. Ruppert, S. Scherer, and H. Stöcker, <i>Phys. Lett. B</i> 575, 85 (2003).</p> <p>[5] A. F. Ali, S. Das, and E. C. Vagenas, <i>Phys. Lett. B</i> 678, 497 (2009).</p> <p>[6] A. Kempf, G. Mangano, and R. B. Mann, <i>Phys. Rev. D</i> 52, 1108 (1995).</p> <p>[7] M. Moshinsky, <i>Phys. Rev.</i> 88, 625 (1952).</p> <p>[8] A. del Campo, G. García-Calderón, and J. G. Muga, <i>Phys. Rep.</i> 476, 1 (2009).</p> <p>[9] G. M. Hossain, V. Husain, and S. S. Seahra, <i>Phys. Rev. D</i> 82, 124032 (2010).</p> | <p>[10] S. S. Seahra, I. A. Brown, G. M. Hossain, and V. Husain, <i>J. Cosmol. Astropart. Phys.</i> 12 (2012) 041.</p> <p>[11] A. Corichi, T. Vukašinak, and J. A. Zapata, <i>Phys. Rev. D</i> 76, 044016 (2007).</p> <p>[12] A. Ashtekar, S. Fairhurst, and J. L. Willis, <i>Classical Quantum Gravity</i> 20, 1031 (2003).</p> <p>[13] E. Flores-González, H. A. Morales-Técotl, and J. D. Reyes, <i>Ann. Phys. (Amsterdam)</i> 336, 394 (2013).</p> <p>[14] J. Bernal, A. Martín-Ruiz, and J. García-Melgarejo, <i>J. Mod. Phys.</i> 4, 108 (2013).</p> <p>[15] A. Martín-Ruiz, J. Bernal, and A. Carbajal-Domínguez, <i>J. Mod. Phys.</i> 5, 44 (2014).</p> <p>[16] I. S. Gradshteyn and I. M. Ryzhik, <i>Table of Integrals, Series, and Products</i>, edited by A. Jeffrey and D. Zwillinger, 4th ed. (Academic Press, New York, 1994).</p> <p>[17] A. Couvert, M. Jeppesen, T. Kawalec, G. Reinaudi, R. Mathevet, and D. Guery-Odelin, <i>Europhys. Lett.</i> 83, 50001 (2008).</p> |
|--|---|

- [18] J. Goldemberg and H. M. Nussensveig, *Rev. Mex. Fis.* **VI.3**, 117 (1957).
- [19] A. Steane, P. Szniftgiser, P. Desbiolles, and J. Dalibard, *Phys. Rev. Lett.* **74**, 4972 (1995).
- [20] P. Szniftgiser, D. Guéry-Odelin, M. Arndt, and J. Dalibard, *Phys. Rev. Lett.* **77**, 4 (1996).
- [21] G. N. Watson, *A Treatise on the Theory of Bessel Functions*, 2nd ed. (Cambridge University Press, Cambridge, UK, 1994), p. 192.
- [22] E. T. Whittaker and G. N. Watson, *A Course of Modern Analysis*, 4th ed. (Cambridge University Press, Cambridge, UK, 1927).
- [23] G. M. Hossain, V. Husain, and S. S. Seahra, *Classical Quantum Gravity* **27**, 165013 (2010).
- [24] M. Moshinsky, *Am. J. Phys.* **44**, 1037 (1976).
- [25] Y. Tamiaki, *Prog. Theor. Phys.* **103**, 1081 (2000).
- [26] J. D. Jackson, *Classical Electrodynamics*, 3rd ed. (Wiley, New York, 1998).